Can we obtain the coefficient of restitution from the sound of a bouncing ball?

Michael Heckel,[1] Aldo Glielmo,[2,1] Nina Gunkelmann,[1,3] and Thorsten Pöschel[1,*]
[1]*Institute for Multiscale Simulations, Friedrich-Alexander-Universität, Erlangen, Germany*
[2]*Physics Department, King's College London, Strand, London WC2R 2LS, United Kingdom*
[3]*Physics Department and Research Center OPTIMAS, University Kaiserslautern, Erwin-Schrödinger-Straße, D-67663 Kaiserslautern, Germany*
(Received 13 November 2015; published 1 March 2016)

The coefficient of restitution may be determined from the sound signal emitted by a sphere bouncing repeatedly off the ground. Although there is a large number of publications exploiting this method, so far, there is no quantitative discussion of the error related to this type of measurement. Analyzing the main error sources, we find that even tiny deviations of the shape from the perfect sphere may lead to substantial errors that dominate the overall error of the measurement. Therefore, we come to the conclusion that the well-established method to measure the coefficient of restitution through the emitted sound is applicable only for the case of nearly perfect spheres. For larger falling height, air drag may lead to considerable error, too.

DOI: 10.1103/PhysRevE.93.032901

I. INTRODUCTION

The coefficient of restitution characterizes the degree of inelasticity of colliding particles. It is of great importance as it is the foundation of both granular hydrodynamics and kinetic theory of granular gases [1,2] as well as event-driven particle simulation of granular matter [3]. In a somewhat simplified version, considered in this paper, it characterizes the inelastic collision of a sphere impacting a plane, where the coefficient of restitution is defined by

$$\varepsilon = -\frac{v'}{v}, \tag{1}$$

where v and v' are the components of the velocity of the sphere normal to the plane before and after the impact, respectively.

The definition, Eq. (1), goes back to Newton [4] and since then the coefficient of restitution and its dependence on material properties, particle size, and impact velocity was under permanent debate, e.g., Refs. [5,6]. A critical review on the early literature can be found in Refs. [7,8].

There is a large body of literature regarding the experimental measurement of the coefficient of restitution, using different techniques, such as high-speed photography [9–11], pendulum systems [12–14], LASER Doppler velocimetry [15], particle-tracking velocimetry [16], and others [17,18]. The most prominent technique exploits, however, the time lag between consecutive impacts of a particle bouncing repeatedly on a horizontal plane:

$$\varepsilon_i = \left|\frac{v_i'}{v_i}\right| = \left|\frac{v_{i+1}}{v_i}\right| = \frac{t_{i+1}-t_i}{t_i - t_{i-1}},$$
$$v_i = \frac{g}{2}(t_i - t_{i-1}) = \frac{g}{2}\Delta t_i, \quad i = 2,3,\ldots. \tag{2}$$

Here, v_i and v_i' are the normal pre- and postcollisional velocities of the ith impact occurring at time t_i, and $g = -9.81\,\mathrm{m/s^2}$ is the gravitational acceleration. This way, from a sequence $t_1, t_2, \ldots, t_N$ we obtain $N-2$ measurements of the coefficient of restitution for specific values of the impact velocity. In Eq. (2), we have assumed a reference frame with the vertical axis pointing upwards; this convention will be used for the rest of this work. The measurement of the coefficient of restitution is, thus, reduced to the measurement of the times t_i determined from the sound emitted due to the collisions, using microphones or acceleration sensors. This technique is, obviously, of striking simplicity and therefore applied extensively for scientific as well as educational purposes, e.g., Refs. [19–35] and many others.

In several references, the precision of this technique was praised, e.g., in Ref. [31] where its accuracy was even claimed explicitly in the title. Surprisingly, however, despite the great popularity of this method, by now there is no detailed error analysis related to this type of measurement, beyond the analysis of the standard deviation computed from the data, thus, quantifying the statistical error [21,23,34,35]. Therefore, in the present paper we analyze the error of the coefficient of restitution measured by means of the described technique. We will show that for typical setups, the error of the measurement of the dissipated energy due to a collision may be as large as 50%.

Albeit historically the coefficient of restitution, ε, was defined by Eq. (1), the quantity of physical interest is rather $(1-\varepsilon)$ or $(1-\varepsilon^2)$ since the latter expressions characterize the dissipation due to inelastic impact and, thus, quantify the system's deviation from the trivial behavior, i.e., perfectly elastic rebound. Therefore, it might be more appropriate to relate the error of a measurement, σ_ε, to $1-\varepsilon$ rather than to ε. We will return to this point in Sec. IV.

II. EXPERIMENT

The experimental setup is sketched in Fig. 1: A small vertical glass tube connected to a vacuum pump via a flexible hose is attached to a robotic arm movable in all three spatial directions. In the beginning of each experiment, a steel sphere of radius $R = 3\,\mathrm{mm}$ and mass $m = 0.9\,\mathrm{g}$ resides at a specified position on a massive glass plate of size $(30 \times 20 \times 1.9)\,\mathrm{cm^3}$. From there, the sphere is picked up, that is, it is suspended at

*thorsten.poeschel@fau.de

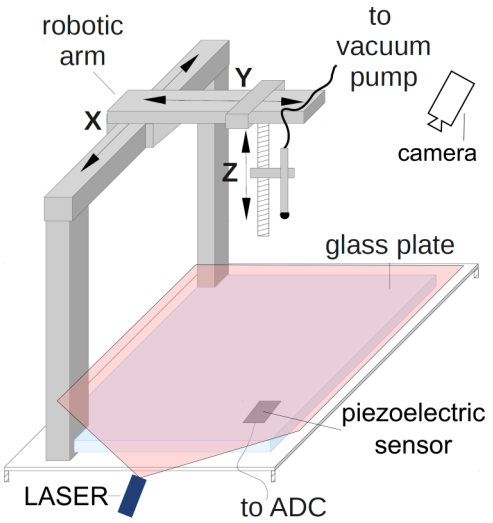

FIG. 1. Schematic diagram of the experimental setup.

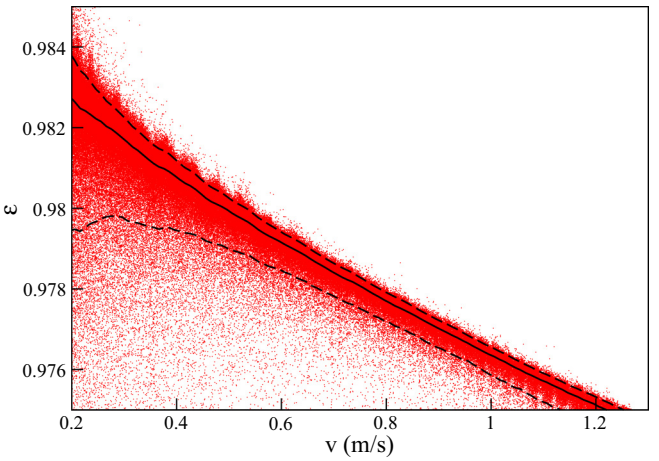

FIG. 2. Coefficient of restitution as a function of the impact velocity. Each of the approximately 280 000 data points corresponds to an impact. The lines shows the median (full line) and the 90 % quantile (dashed lines).

the lower end of the tube by means of vacuum. The robot moves the sphere then to a desired position $\{x,y,z\}$. By switching off the vacuum pump, the sphere is released to bounce repeatedly off the ground. When the ball eventually comes to rest, it is pushed to a defined position by a fan, from where the robot picks it up again. Sound emission caused by the impacts is detected by a piezoelectric sensor (EKULIT EPZ-Piezoelectric ceramic element with characteristic frequency 18 kHz). The sensor was mounted on the lower side of the plate, 5 cm away from the corner, and recorded by a computer; see Sec. III B. A LASER sheet oriented parallel to the plate in distance of slightly more than the sphere diameter and a camera were used to determine the location of the impact; see Sec. III C.

The initial horizontal (x,y) position is chosen randomly within the central region of the ground plate for each cycle. Edge effects [36] are, therefore, not noticeable. The initial impact velocity is randomly chosen from $v \in (1.33,1.4)$ m/s (corresponding to $z \in (9,10)$ cm), resulting in 90–100 bounces of the ball in each trial. This way, via Eq. (2), we perform about 6 000 measurements of $\varepsilon(v)$ per hour. To assure stationary conditions, the experiment was performed in a climate chamber to keep temperature and humidity of the experimental environment at constant values. The experiment was performed in darkness with the only illumination from the LASER sheet to conveniently determine the locations of the impacts from the reflections of the LASER at the sphere's surface; see Sec. III C. Figure 2 shows the coefficient of restitution as a function of the impact velocity, for the system described above. The figure shows about 280 000 data points. For the statistical analysis we neglected the first 10^4 bounces in order to suppress effects due to initial wear; see Sec. III E. The characteristic frequency of the sensor is far away from the frequency of flexural oscillations of the base plate (96.2 Hz; see Ref. [37]). Therefore, we can exclude that the sound signal is due to flexural oscillations of the base plate whose propagation speed might depend on the velocity of the impact. Further information regarding the details of the experimental setup will be given below in relation to the estimation of experimental errors.

III. ESTIMATION OF THE EXPERIMENTAL ERRORS

A. Main sources of errors

The results obtained from the experiment described above are affected by different kinds of imperfections, resulting in experimental uncertainty and, thus, errors. We identified the following imperfections as putative main sources of errors:

- uncertainty of the time of impact by measuring the emitted sound
- different location of consecutive impacts
- air drag
- wear of the plate and the sphere in long-time experiments
- imperfection of the spherical shape with respect to surface roughness
- imperfection of the spherical shape with respect to eccentricity

In the following sections, we consider the above itemized sources of error in detail.

Besides the mentioned sources of error, fluctuations of the humidity may contribute to the uncertainty of the measurement as humidity influences the contact forces between the surface and the sphere. Fluctuations of temperature would change the material stiffness of the plate and the sphere. We disregard these sources of error here, since the experiment was performed in a climate controlled chamber such that no influence of variations of temperature or humidity was apparent.

When quantifying the error, we should keep in mind that the inelastic nature of a collision is not characterized by the coefficient of restitution, ε, but rather by the deviation of the (trivial) elastic case, $(1-\varepsilon)$. Therefore, an experimental error should be better related to $(1-\varepsilon)$. We will see below that an experimental error that appears acceptable when related to ε can lead to very large relative errors of $(1-\varepsilon)$.

B. Uncertainty of the time of impact

The experimental method relies on the precise measurement of the impact times [see Eq. (2)], which is affected by experimental errors. There are two factors of different nature

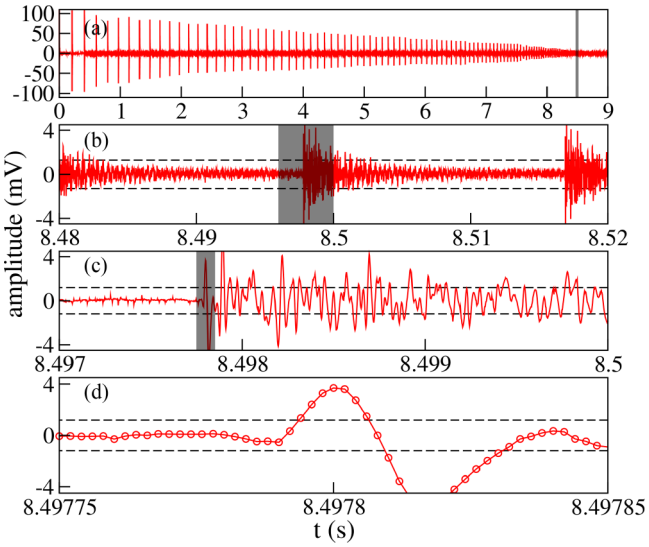

FIG. 3. Sound signal measured by the piezoelectric sensor in different resolution. Gray shaded areas in panels (a)–(c) indicate the time interval displayed in the subsequent panel of higher resolution, panels (b)–(d). (a) Full signal corresponding to one drop and approximately 100 subsequent bounces; (b) sound due to a single bounce at $t \approx 8.498$ s. The next impact occurs at $t \approx 8.518$ s; (c) sound at the beginning of an impact; (d) high resolution where discrete sample points are shown with symbols. Dashed lines show the thresholds, $V_{\rm thr}$, used for the impact recognition. In this case, the impact was recognized about two sample intervals after the physical contact, corresponding to a delay of 4 μs.

limiting the precision of the measurement: (a) the precision of the (digital) clock, and (b) the criterion by which an impact is detected.

The signal from the piezoelectric sensor was processed using an AD converter (NI PCIe-6251) with 16-bit signal resolution sampled at $5 \times 10^5\,{\rm s}^{-1}$, which results in a time resolution of 2 μs. We will see below that the error due to the finite time resolution is subdominant to the uncertainty related to (b).

Consider now (b), the criterion by which an impact is detected: Fig. 3 shows the sound signal of one particle drop, where the particle bounces approximately 100 times.

In low resolution, Fig. 3(a), we see that the impacts can be well separated in the sound signal due to a high signal-to-noise ratio and steep gradient at the beginning of an impact. The sudden jump in the signal amplitude apparent in Fig. 3(b) occurs in far less than a millisecond. In high resolution, Figs. 3(c) and 3(d), we see, however, that the amplitude of the signal at the beginning of an impact does not rise abruptly but gradually at the scale of the time interval between contiguous samples. Therefore, in order to determine the time of an impact, we need a criterion that takes into account both the finite noise level and the gradual rise of the sound signal emitted when the sphere touches the plane.

We *defined* the time of an impact, t_i, as the time when the signal exceeded a threshold $V_{\rm thr}$, which has to be chosen with some care: The threshold should be significantly larger than the noise level $|V_{\rm thr}| > |V_{\rm noise}|$. On the other hand, a low threshold is needed to record a long sequence of bounces for each drop. Moreover, the value of the threshold determines the delay between the physical impact and its identification and, thus, the error of the measurement. In our experiment, we measured a noise level of about $|V_{\rm noise}| \lesssim 1\,\mu$V. Assuming a threshold $V_{\rm thr} = 1$ mV as a criterion for the start of an impact we could safely distinguish 80–100 consecutive bounces. After approximately 100 bounces, the signal-to-noise ratio turned too small to allow for a reliable measurement.

By visual inspection of about 50 signals due to impacts close to the end of the sequence of bounces for several drop experiments, we found the delay between the impact and the time when the corresponding voltage exceeds $V_{\rm thr}$ always less than 5 sample points. An example is given in Fig. 3(d), where the high resolution allows us to inspect the single data points. Consequently, the error of the measurement of t_i is bound by $\Delta_t = 10\,\mu$s. The mean delay of all inspected signals was 1.6 sample points corresponding to $\approx 3\,\mu$s.

To compute the error due to the uncertainty of the impact times, t_i, we consider the coefficient of restitution as given by Eq. (2) as a function of the measured times, $\varepsilon = \varepsilon(t_{i-1}, t_i, t_{i+1})$:

$$\sigma_{\varepsilon,i} = \sqrt{\left(\frac{\partial \varepsilon_i}{\partial t_{i-1}}\Delta_t\right)^2 + \left(\frac{\partial \varepsilon_i}{\partial t_i}\Delta_t\right)^2 + \left(\frac{\partial \varepsilon_i}{\partial t_{i+1}}\Delta_t\right)^2}$$
$$= -\,\Delta_t \frac{g}{2v_i^2}\sqrt{v_{i+1}^2 + (v_{i+1}+v_i)^2 + v_i^2}. \qquad (3)$$

Note that g was defined with a negative sign. In agreement with Fig. 2, $\sigma_{\varepsilon,i}$ increases for low velocities. This can be also seen writing Eq. (3) in the form

$$\sigma_{\varepsilon,i} = -\,\Delta_t \frac{g}{2v_i}\sqrt{\frac{v_{i+1}^2}{v_i^2} + \left(\frac{v_{i+1}}{v_i}+1\right)^2 + 1}$$
$$= -\,\Delta_t \frac{g}{\sqrt{2}}\frac{\sqrt{\varepsilon_i^2 + \varepsilon_i + 1}}{v_i}. \qquad (4)$$

For large i, ε_i approaches unity whereas the impact velocity, v_i, decays to small values. Therefore, the standard deviation, $\sigma_{\varepsilon,i}$, becomes large for large impact counter, i. Hence, the largest error is obtained at small velocities $v_i \approx 0.2$ m/s and, with $\varepsilon_i \approx 0.98$, we obtain $\sigma_{\varepsilon,i} \approx 6 \times 10^{-4}$.

C. Different location of consecutive impacts

The sound signal emerging at the point of the impact needs some time to reach the piezoelectric sensor mounted close to the corner of the plate to its lower side, due to the finite speed of sound in the plate material. This delay would not affect the measurement if the points of impact would be the same for all bounces since only differences of times, $t_{i+1} - t_i$, enter Eq. (2). Therefore, the error is due to the distance of the location of consecutive impacts.

In order to estimate the corresponding error, we attached a second piezoelectric sensor close to the opposite side of the plate and recorded both signals simultaneously. Choosing the initial point of impact such that the difference of the distances to both sensors is about 10 cm, we obtained a delay of 18 μs between the signals corresponding to the speed of sound 5.5×10^3 m/s in the glass plate. When we determine the coefficient of restitution due to Eqs. (2) independently by using

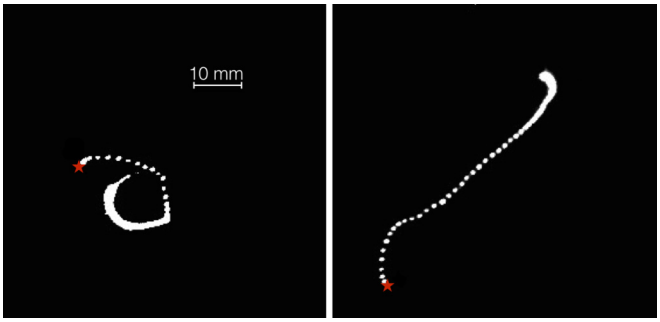

FIG. 4. Two typical images obtained by long-time exposure. When the sphere crosses the LASER sheet, the sphere's reflection indicates the spacial location of its impacts on the glass plate. A star indicates the position of the first impact. Reflections of the spots from the glass plate were removed by digital post-processing.

the signals from both sensors, the difference, $\varepsilon^1 - \varepsilon^2$, does not show systematic deviations beyond very small statistical fluctuations. In particular, we do not see a dependence of $\varepsilon^1 - \varepsilon^2$ as a function of the location of the impact, that is, the difference of the distances of the point of impact from the locations of the sensors. This may be considered as further evidence for the fact that the details of sound transmission from the point of impact to the locations of the sensors is irrelevant for the measurement.

To determine the locations of the impacts, we used a LASER sheet oriented parallel to the plate (see Fig. 1) and in distance 7 mm to the plate, which is slightly more than the particle diameter. Therefore, immediately before the particle impacts the plate, the LASER was reflected by the sphere's surface in vertical direction and the corresponding flash was recorded by a camera located about 1 m above the plate. The camera's shutter was opened for the duration of 10 s starting at the time when the sphere was released from the vacuum tube, such that the locations of the impacts could be identified for the sequence of bounces. The sequence terminates when the height of the jumps drops below 1 mm such that the upper surface cannot cross the LASER sheet. Figure 4 shows an example image.

Analyzing these data we found that (a) the distance of consecutive bounces decays rapidly with the impact counter. The largest leaps in horizontal direction occur within the very first bounces, and (b) in no case, the distance between consecutive impact points was larger than 5 mm.

From these observations, we conclude that the maximum uncertainty of the measured time differences due to different location of consecutive impacts is $\Delta_{\Delta t} \approx 5\,\mathrm{mm}/5.5 \times 10^3\,\mathrm{m/s} \approx 0.9\,\mu\mathrm{s}$. This yields an error on $\varepsilon = \varepsilon(\Delta t_i, \Delta t_{i+1})$ calculated as

$$\sigma_{\varepsilon,i} = \sqrt{\left(\frac{\partial \varepsilon_i}{\partial \Delta t_i}\Delta_{\Delta t}\right)^2 + \left(\frac{\partial \varepsilon_i}{\partial \Delta t_{i+1}}\Delta_{\Delta t}\right)^2} = -\Delta_{\Delta t}\frac{g}{2}\frac{\sqrt{\varepsilon_i^2+1}}{v_i}. \tag{5}$$

Again the uncertainty is maximized at small impact velocities. For $v_i \approx 0.2\,\mathrm{m/s}$ and $\varepsilon_i \approx 0.98$ this is found to be $\sigma_{\varepsilon,i} \approx 3 \times 10^{-5}$.

D. Influence of air drag

When computing the coefficient of restitution according to Eq. (2), we assume that the postcollisional velocity of collision $i-1$ equals the impact velocity of collision i, up to the sign

$$v_i = -v_{i-1}', \tag{6}$$

which neglects the effect of air drag during the free flight. Indeed, the true impact velocity is slightly smaller by absolute value,

$$v_i^{\mathrm{air}} < -v_{i-1}', \tag{7}$$

which leads to an underestimation of the coefficient of restitution. Note that in difference to all other sources of error discussed in this paper, this error is systematic. However, it is common to compare random and systematic uncertainties to obtain the overall measurement error [38]. Denoting the coefficient of restitution corresponding to v_i^{air} by $\varepsilon_i^{\mathrm{air}}$, the relative error is defined as the ratio of the absolute error $\varepsilon_i^{\mathrm{air}} - \varepsilon_i$ and the quantity $\varepsilon_i^{\mathrm{air}}$ [38]:

$$\Delta\varepsilon^{\mathrm{air}}(v_i^{\mathrm{air}}) = \frac{\varepsilon_i^{\mathrm{air}} - \varepsilon_i}{\varepsilon_i^{\mathrm{air}}} = 1 - \frac{v_i'}{v_{i-1}'}\left[-\frac{v_i'}{v_i^{\mathrm{air}}}\right]^{-1} = 1 + \frac{v_i^{\mathrm{air}}}{v_{i-1}'}. \tag{8}$$

In order to estimate the error $\Delta\varepsilon^{\mathrm{air}}$, we compute the velocity of the next collision, v_i^{air}, of a particle rebouncing at velocity v_{i-1}'.

Given the initial impact velocity $v \approx 1.38\,\mathrm{m/s}$, resulting from the dropping height of $\approx 10\,\mathrm{cm}$, the maximal Reynolds number is

$$\mathrm{Re} = \frac{\rho v L}{\eta} \approx 629, \tag{9}$$

where $\rho = 1.3\,\mathrm{kg/m^3}$ is the density of air, $L = 2R = 6\,\mathrm{mm}$ is the characteristic length and $\eta = 17.1\,\mu\mathrm{Pa\,s}$ is the dynamic viscosity of air. For $\mathrm{Re} \lesssim 1$, the flow is laminar, such that Stokes drag force applies and for $\mathrm{Re} \gtrsim 500$, Newton's drag law is in order. Since the motion is not clearly laminar nor turbulent, we consider both types of drag and assume the maximum resulting error for the coefficient of restitution.

The equations of motion between the impacts are, thus,

$$\ddot{z} - g + \alpha_S \dot{z} = 0, \quad \alpha_S \equiv \frac{6\pi R\eta}{m}, \tag{10a}$$

$$\ddot{z} - g + \alpha_N \frac{\dot{z}}{|\dot{z}|}\dot{z}^2 = 0, \quad \alpha_N \equiv \frac{C_d \rho \pi R^2}{2m}, \tag{10b}$$

where $C_d = 0.47$ is the drag coefficient of a sphere and $g = -9.81\,\mathrm{m/s^2}$ is gravity. Equation (10a) applies to Stokes drag and Eq. (10b) to Newton drag.

Consider first Stokes drag. For convenience we assume that the table is located at $z = -R$ such that the impact takes place when the center of the sphere is at $z = 0$. Solving Eq. (10a) with initial conditions $z(0) = 0$ and $\dot{z}(0) = v_{i-1}'$ gives

$$z(t) = \frac{gA_S}{\alpha_S^2}(e^{-\alpha_S t} - 1) + \frac{gt}{\alpha_S}, \tag{11}$$

where

$$A_S \equiv \frac{g - \alpha_S v_{i-1}'}{g} \tag{12}$$

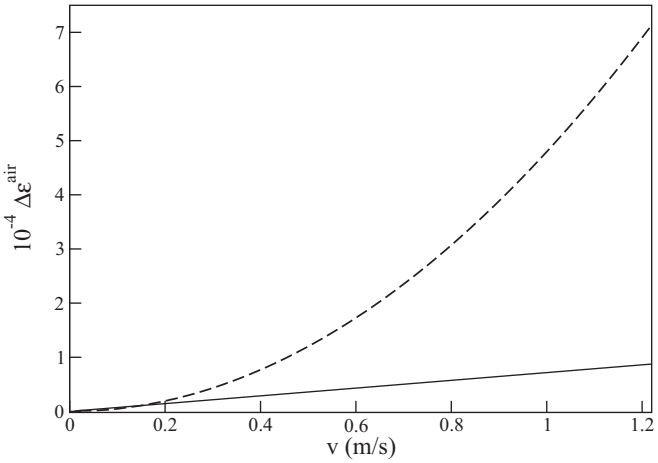

FIG. 5. Relative error of the coefficient of restitution due to air drag [Eq. (8)], as a function of impact velocity. Full line, with the assumption of Stokes drag, Eq. (10a); dashed line, with the assumption of Newton drag, Eq. (10b).

characterizes the drag force as compared to the weight of the particle. The corresponding velocity reads

$$\dot{z}(t) = \frac{g}{\alpha_S}(1 - A_S\, e^{-\alpha_S t}). \tag{13}$$

From Eq. (11) we obtain the time of the next impact t_i by $z(t_i) = 0$,

$$t_i = \frac{1}{\alpha_S}[\mathcal{W}(-A_S e^{-A_S}) + A_S], \tag{14}$$

where Lambert's function, $\mathcal{W}(x)$, is the solution of $\mathcal{W}(x)\exp\mathcal{W}(x) = x$.

Inserting Eq. (14) into Eq. (13) one obtains the impact velocity, $v_i^{\rm air} = \dot{z}(t_i)$. Finally, using Eq. (8), the error due to the air drag is calculated. For the range of parameters considered, this can be well approximated with a first-order Taylor expansion around $\alpha_S = 0$, which gives

$$\Delta\varepsilon^{\rm air} = -\frac{2\alpha_S v'_{i-1}}{3g}. \tag{15}$$

The systematic error due to the air drag as a function of the impact velocity is shown in Fig. 5 and it is bound by $\Delta\varepsilon^{\rm air} < 9\times10^{-5}$.

The same calculation can be done with the assumption of Newton drag. This time Eq. (10b) has to be solved separately for the upwards and downwards motion of the sphere, in order to easily take into account the different sign of the drag force. The resulting error is again approximated to first order in α_N to give

$$\Delta\varepsilon^{\rm air} = -\frac{\alpha_N v'^2_{i-1}}{2g}\,, \tag{16}$$

which is also shown in Fig. 5 (dashed line) as a function of impact velocity. Thus, for the case of Newton drag, for our parameters we obtain $\Delta\varepsilon^{\rm air} \lesssim 7\times10^{-4}$. For details of the calculation see Ref. [39].

In conclusion we see that in the relevant interval of impact velocity, for both cases Newton drag and Stokes drag the systematic error due to air resistance is $\Delta\varepsilon^{\rm air} \lesssim 7\times10^{-4}$.

E. Wear of the plate and the sphere

When designing an automated bouncing ball experiment, there are two fundamentally different layouts: Type (a) uses a reservoir of identical spheres and releases one after the other to record the noise emitted from their bounces. Type (b) uses a single sphere that is released, bounces on the plate until it comes to rest, and is then transported back to the starting position. The layout of type (a) is technically simpler; however, there is an additional source of error originating from the statistical distribution of the mechanical properties of the spheres. Type (b) is free of this error; however, a possible drift of the results due to wear of the ball and the plate should be considered given that the sphere suffered from up to $\sim 10^6$ violent bounces.

We analyzed the surface of the sphere by means of a scanning electron microscope (SEM) before the experiment and in regular intervals of about 10^5 bounces. As a result, except for the initial period of about 10^5 bounces, no significant wear was observed. Figures 6(a) and 6(b) show SEM pictures of the sphere before the experiment and after about 10^5 impacts where only very minor damages of the surface are visible. Figures 6(c)–6(e) show magnifications of the sphere's surface after 0, 10^5, and 10^6 impacts. The shown region covers about 1.8% of the contact area for a collision starting at height 10 cm. While the number of tiny scratches on the sphere's surface increased initially, the surface structure saturated quickly such that we did not notice further roughening due to repeated impacts of the sphere. The structure of the surface remains approximately invariant. A very similar analysis was done to investigate damages of the plate but no sign of roughening was found. Therefore, possibly except for the initial period, we exclude errors and in particular a systematic drift due to wear of the sphere or the plate.

As further evidence, in Fig. 7(a) we replot the data shown in Fig. 2, $\varepsilon(v)$ (median value), where we analyze the first 10^4 impacts, the last 10^4 impacts and the full set of impacts separately.

Figure 7(b) shows the histogram of measured data for fixed impact velocity, $v = (0.7 \pm 0.05)$ m/s, characterizing the fluctuations. Again, three sets of data correspond to separate analysis of the first 10^4 impacts, the last 10^4 impacts and the full data set. Except for larger scatter of the restricted sets, due to smaller amount of data, all three sets lead to the same statistics up to fluctuations. No systematic trend due to wear was apparent.

F. Imperfections of the spherical shape

1. *Classification and method*

The coefficient of restitution describes the change of relative velocity of the particle and the plate in normal direction *at the point of contact*. Therefore, bouncing-ball experiments as described in Sec. II are only useful to determine the coefficient of restitution if the bouncing body is a sphere. Surprisingly, this simple but important detail is rarely mentioned in the literature. Deviations from the spherical shape will lead to sizable errors of the measured coefficient of restitution. In this section, we discuss the error due to imperfections of two different types: (a) surface roughness,

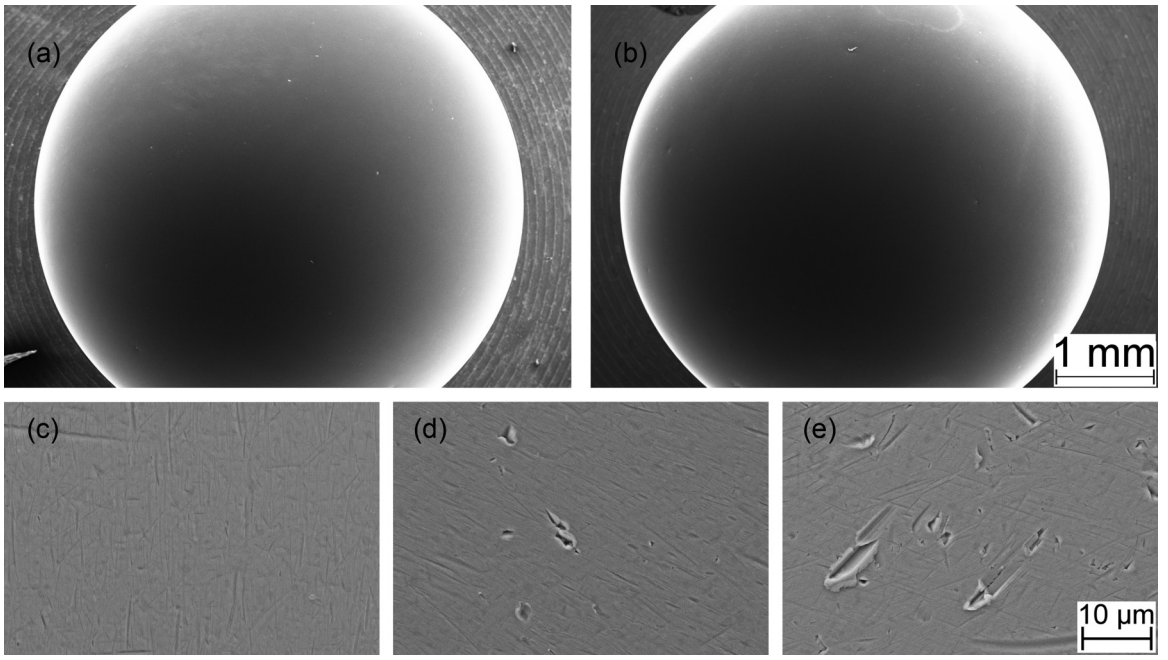

FIG. 6. SEM pictures of the sphere. (a) before the experiment (0 impacts) and (b) after 10^5 impacts. Only very small scratches at the surface are noticeable. Panels (c)–(e) show magnifications of the surface, (c) before the experiment (0 impacts), (d) after about 10^5 impacts, (e) toward the end of the experiment after about 10^6 impacts. Very small scratches are noticeable. The region shown in each image covers about 1.8% of the contact area for a collision starting at height 0.1 m.

that is, small scale impurities of the surface, and (b) eccentricity, that is, deviations of the overall shape from the perfect sphere.

Since there is no experimental means to individually control these deviations, we use a numerical simulation to estimate the corresponding errors. We describe the imperfect sphere by means of a mechanical model whose validity was confirmed by direct comparison with experimental data [40]. By varying the characteristics of the simulated particle we are able to isolate imperfections of type (a), Sec. III F 2, and (b), Sec. III F 3, from all other sources of error.

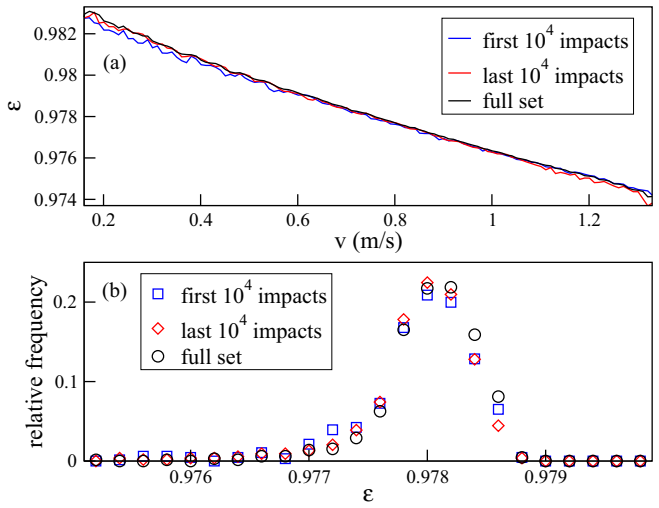

FIG. 7. (a) Replot of Fig. 2 [only median of $\varepsilon(v)$], where we analyze the data from the first and last 10^4 impacts separately. (b) Histogram of the measured data for a particular velocity, $v = (0.7 \pm 0.05)\,\mathrm{m/s}$. In both figures (a, b), no systematic trend is apparent.

2. *Surface roughness*

In a recent model [40] a rough sphere was modeled by a central (perfect) sphere and a large number (several millions) of microscopic spherical asperities located at random positions at the sphere's surface (Fig. 8).

The contact between the particle and the plane occurs, thus, via one of the asperities. The local change of velocity at the point of contact is then described by a *microscopic* coefficient of restitution, $\epsilon(v_c)$, which was derived analytically for the viscoelastic collision of a perfect sphere with a plane [41–43] at normal velocity v_c at the point of contact. For the simulation we represented the microscopic coefficient of restitution by means of a convergent Padé approximant of order [1/4], for

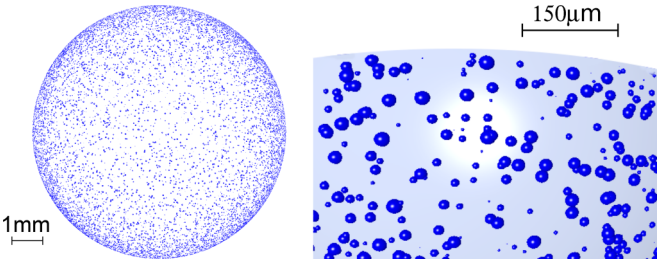

FIG. 8. Numerical model of a rough sphere [40], where a large number of tiny spheres is attached to random positions at the surface of a large central (perfect) sphere. For visibility, the number of asperities is much smaller than in the simulation. For the same reason, the size of the asperities is not to scale.

details see Refs. [44,45]:

$$\epsilon(v_c) \approx \frac{1 + c_1 v_{c_*}}{1 + b_1 v_{c_*} + b_2 v_{c_*}^2 + b_3 v_{c_*}^3 + b_4 v_{c_*}^4}, \qquad v_{c_*} = \beta^{1/2} v_c^{1/10}, \tag{17}$$

with the universal (material independent) constants $c_1 = 0.501086$, $b_1 = 0.501086$, $b_2 = 1.15345$, $b_3 = 0.577977$, $b_4 = 0.532178$. The material constant $\beta = 0.0467$ was determined by fitting Eq. (17) to the experimental data; see Ref. [40].

In numerical experiments we released the particle from a certain height just as in the experiment described above and simulated the sequence of collision in analogy to the experiment. When the particle contacts the plane through one of its asperities, we compute the local change of velocity due to the impact geometry and the microscopic coefficient of restitution, to obtain the impulse on the particle at each impact. These impulses govern the dynamics of the particle in an event-driven molecular dynamics simulation. Micromechanically, when the particle collides with the plane, there act torques due to the asperities which cause transfer between the translational and rotational degrees of freedom. Since the rotation of the particle does not influence the coefficient of restitution determined via Eq. (1), the rotational degrees of freedom act like a reservoir of energy and at each collision a certain amount of energy is exchanged between the rotational and translational degrees of freedom. The amount depends on the details of the contact mechanics, that is, on the angular orientation of the particle at the instant of the contact and on the positions of the asperities, which may be considered as random variables, thus appearing like an uncertainty of measurement. It was shown that the coefficient of restitution obtained from numerical simulations of the described model reveals the same characteristics as the experimental results. This concerns both mean values of the function, $\varepsilon(v)$, and also the statistical characteristics of the data [40,46]. Figure 9 shows the coefficient of restitution obtained from a numerical simulation. Here the central sphere of radius $R = 3$ mm was covered by 3×10^6 asperities of size $R_i \leqslant R \times 10^{-3}$.

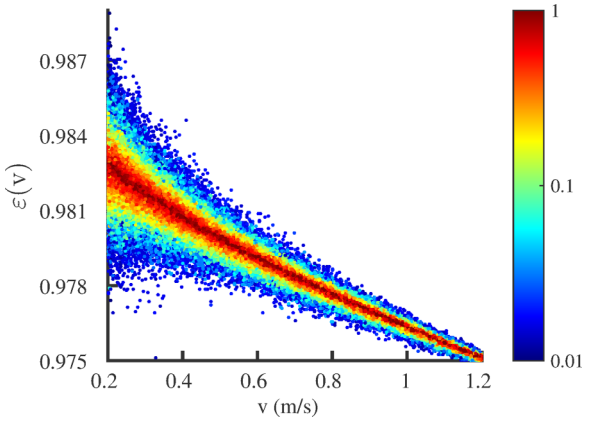

FIG. 9. Coefficient of restitution for a rough particle plotted against the impact velocity. The data are colored according to the normalized frequency of occurrence.

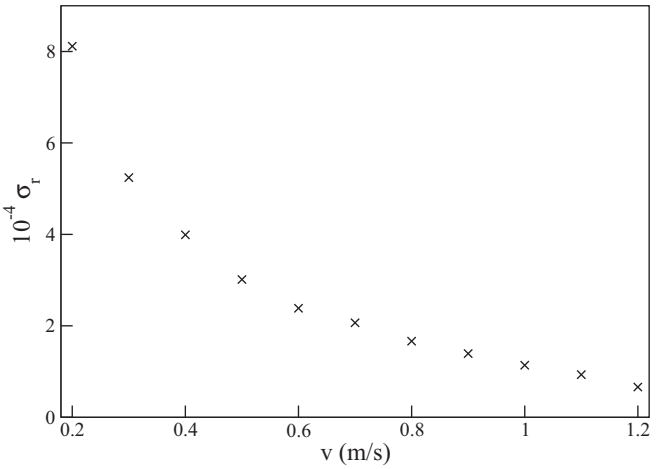

FIG. 10. Standard deviation of the data shown in Fig. 9 computed due to Eqs. (18), as a function of impact velocity.

Having the experimental data sufficiently closely reproduced, the error due to roughness can be determined from the standard deviation of the data, isolated from other sources of experimental error. The error as a function of the impact velocity is determined by

$$\sigma_r(v) = \sqrt{\frac{1}{n(v)} \sum_{i=1}^{n(v)} [\varepsilon_i - \overline{\varepsilon}(v)]^2}, \qquad \overline{\varepsilon}(v) = \frac{1}{n(v)} \sum_{i=1}^{n(v)} \varepsilon_i, \tag{18}$$

where the sum is performed over all data points (ε_i, v_i) where $|v - v_i| < \delta_v$ and $n(v)$ is the number of such data points. The value of δ_v must be chosen with care since it compromises between good statistics (large δ_v) and good v resolution (small δ_v); here we use $\delta_v = 0.01$ m/s. Figure 10 shows the standard deviation of the data shown in Fig. 9 due to Eqs. (18), as a function of impact velocity, $\sigma_r(v)$. We observe that the standard deviation σ_r increases for small impact velocity.

The particle interaction model, Eq. (17), considers only restitution in normal direction but does not take into account friction. For the justification of this assumption we make the following estimate: Assume N asperities are homogeneously distributed on the surface of the sphere of radius R in close packing. Thus, each sphere may be thought located in the center of a regular hexagon of side length a such that the abundance of hexagons fill the surface area completely. We obtain

$$a = \frac{4}{\sqrt{6}\, 3^{1/4}} \frac{\sqrt{\pi}}{\sqrt{N}} R, \tag{19}$$

and the distance of adjacent asperities,

$$d = \frac{4}{3^{1/4}\sqrt{2}} \frac{\sqrt{\pi}}{\sqrt{N}} R. \tag{20}$$

With the largest possible horizontal distance, $d/2$, between the center of the sphere and the point where one of the asperities touches the plane, the vertical and horizontal components of

the interaction force vector relate as

$$\frac{F_t}{F_n} < \frac{4}{3^{1/4}\sqrt{2}}\frac{\sqrt{\pi}}{\sqrt{N}} \approx 3.81\frac{1}{\sqrt{N}}. \tag{21}$$

Sliding friction becomes active when $F_t \geqslant \mu F_n$ according to the Coulomb friction criterion, where the friction coefficient adopts typical values $0.01 \lesssim \mu \lesssim 1$. Thus, for $N \gtrsim 1.5 \times 10^5$ the particle cannot slide and friction is, therefore, irrelevant.

3. *Eccentricity*

Complementary to surface roughness, that is, deviations from the perfect sphere on a microscopic scale, in this section we consider deviations from the spherical shape on the scale of the particle size, disregarding roughness. To this end, the particle is modeled by two identical spheres of radius R and distance L, with $L \ll R$; see Fig. 11.

Similarly to the previous section, we perform bouncing-body experiments and determine the coefficient of restitution via Eq. (1), in analogy to the experiment [47]. Figure 12 shows the coefficient of restitution obtained from a numerical simulation of 4×10^4 bounces of the particle for two different values of the eccentricity, $L/R = 0.1$. The scatter increases steadily with decreasing impact velocity similar to our observations for rough particles. Again, the reason for the scatter is transfer between the translational and rotational degrees of freedom similar as discussed in the previous section. The amount of the transferred energy depends on the impact velocity and on the angular orientation of the particle at the instant of contact. The orientation may be considered as a random variable, except toward the end of the collision sequence when the height of the jumps approaches the order of L [47]. The randomness of the numerically determined coefficient of restitution characterizes the uncertainty of the measurement due to the deviation of the particle shape from the perfect sphere.

Figure 13 shows the uncertainty of the numerical measurement, quantified by the standard deviation due to Eqs. (18), for eccentricity $L/R = 0.01$ and $L/R = 0.02$ corresponding to high precision glass spheres [48] as frequently used in bouncing ball experiments. Again, the standard deviation σ_r increases for small impact velocity.

Even small deviations from the spherical shape lead to significant errors.

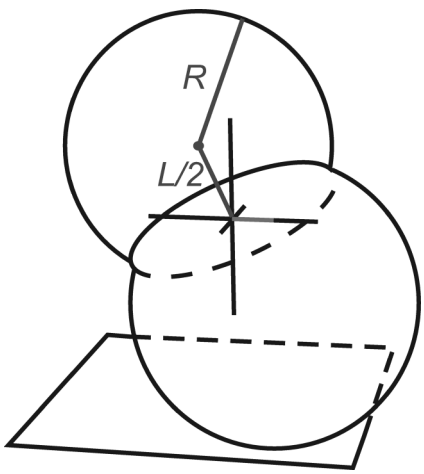

FIG. 11. Sketch of a dumbbell particle consisting of two identical spheres of radius R and distance $L \ll R$. For better visibility, the value of L appears exaggerated.

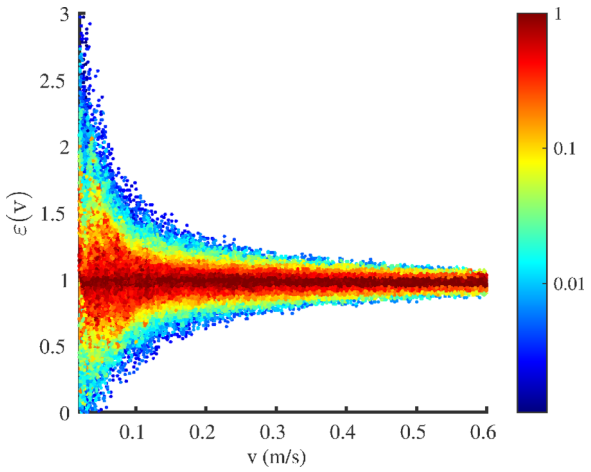

FIG. 12. The coefficient of restitution as a function of velocity for eccentricity $L/R = 0.1$. The data are colored according to the normalized frequency of occurrence.

IV. DISCUSSION

One of the standard methods for measuring the coefficient of restitution relies on the analysis of the sound emission from a ball bouncing recurrently on a solid floor. There is a large body of literature on this method; however, much less is known about the precision and validity of it. In this work we quantified, for the first time, the errors of this widely used experimental method.

The concrete numbers of the experimental error depend, of course, on the specific properties of the experiment, such as particle size, material properties, etc. In this paper, we consider experimental parameters typical to many experiments found in the literature, where the coefficient of restitution was obtained

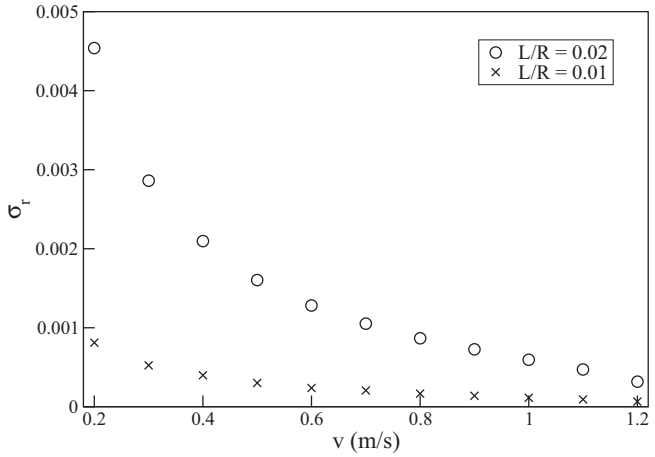

FIG. 13. Standard deviation of the numerically determined coefficient of restitution for eccentricity $L/R = 0.01$ and $L/R = 0.02$, as a function of impact velocity.

TABLE I. Comparison of the sources of error through their induced standard deviations, σ, for impact velocity 0.2 m/s. For the case of air drag, the value of the uncertainty, $\Delta\varepsilon^{\text{air}}$ for impact velocity 1.2 m/s is given. For the full range of velocity, see Fig. 14.

	Error source	Section	σ; $\lvert\Delta\varepsilon\rvert$
(a)	Time of impact	III B	6×10^{-4}
(b)	Location of impact	III C	3×10^{-5}
(c)	Air drag	III D	7×10^{-4}
(d)	Wear	III E	Not noticeable
(e)	Roughness	III F 2	9×10^{-4}
(f)	Asphericity $L/R = 0.01$	III F 3	8×10^{-4}
	Asphericity $L/R = 0.02$	III F 3	4.5×10^{-3}

from the time lag between consecutive impacts of a particle bouncing on a flat plate [13,33–35,49,50].

We investigated the main sources of experimental error, due to (a) the uncertainty of the measurement of time of the impacts, (b) varying location of successive impacts, (c) air drag, (d) wear of the plate and the sphere, (e) roughness of the surface, and (f) eccentricity of the sphere. Other sources of error such as varying temperature and humidity were not considered as the experiment was performed in a climate controlled chamber. Table I shows a comparison of the maximal errors due to these sources, represented by the standard deviation, σ, for impact velocity 0.2 m/s. For the case of air drag (which is the only systematic error), the value of the uncertainty, $|\Delta\varepsilon|$, for impact velocity 1.2 m/s is given.

We conclude that, for all impact velocities considered, the experiment is rather insensitive to wear, uncertainties of the location of impact and time measurements. In contrast, the method is sensitive to deviations from the perfect spherical shape of the particles, that is, roughness and asphericity as well as air drag. Figure 14 shows the total error due to these main contributions for the full range of impact velocity considered.

As a surprising result, we find that the geometrical properties of the particle, that is, its deviation from the perfectly spherical shape dominates the error of the measurement of the coefficient of restitution. Due to our knowledge, this source of error was, so far, not even discussed in the literature. Even for high precision glass beads with typical asphericity of 1...2%, as frequently used in bouncing ball experiments the standard deviation is $\sigma \approx 1 \ldots 5 \times 10^{-3}$.

An even more surprising result is the error due to air drag, which can even exceed the error due to imperfect shape for larger impact velocity. For our set of parameters specified in Sec. II, which is typical for many experiments reported in the literature, for dropping height $h \gtrsim 7$ cm, air drag is the largest contribution to the total error.

An error of $\sigma \approx 10^{-3}$ looks acceptable, at first glance. However, in strict sense, it is not the coefficient of restitution, ε, that quantifies the dissipation of a collision but rather $(1-\varepsilon)$. Typical values for glass or steel spheres at typical impact velocities are $(1-\varepsilon) \approx 0.01 \ldots 0.02$. A standard deviation of 8×10^{-4} for high precision spheres implies a relative error $\sigma/(1-\varepsilon)$ of typical $4 \ldots 8$ %. For slightly less precise spheres, $L/R = 0.02$, with $\sigma \approx 5 \times 10^{-3}$, the relative error of the inelasticity $(1-\varepsilon)$ can easily exceed $20 \ldots 50$ %. The same is true with respect to air drag—most experiments reported in the literature use dropping height of 10–50 cm. From our results, we may conclude, however, that for a typical system (glass or steel spheres) a dropping height of more than about 5 cm renders the results questionable because of large errors due to air drag.

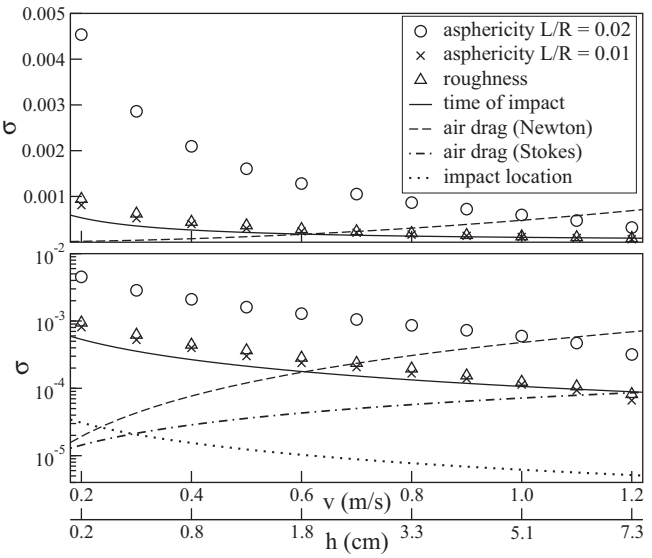

FIG. 14. Top: Contributions to the total error characterized by the standard deviations as a function of impact velocity. Bottom: Same data but in logarithmic scale. For small impact velocity, imperfections of the shape of the ball dominate the total error. For larger impact velocity, $v \gtrsim 1.2$ m/s, corresponding to dropping height $h \gtrsim 7$ cm, the error due to air drag becomes considerable (see second horizontal scale). The given numbers are typical but specific for our set of parameters; see Sec. II.

In conclusion, we found that the details of the shape of the particle are essential for the experimental error. Only particles with very small deviation from the mathematical sphere allow for the measurement of the coefficient of restitution using the sound method at acceptable precision. A second important contribution to the error comes from air drag. We wish to point out that this contribution is a *systematic* error that can be corrected. According to our knowledge this was not done so far in the literature. Aside from that, only the precision of the measurement of the time of impact and the logical identification of impacts from the sound data have significant impact on the precision of the measurement.

ACKNOWLEDGMENTS

We acknowledge funding by Deutsche Forschungsgemeinschaft through the Cluster of Excellence "Engineering of Advanced Materials" and through research Project No. PO472/24-1. We thank Benjamin Butz and Erdmann Spiecker for SEM microscopy. A.G. thanks the Deutsche Akademische Austauschdienst (DAAD) for a RISE scholarship.

[1] I. Goldhirsch, Annu. Rev. Fluid Mech. **35**, 267 (2003).
[2] N. Brilliantov and T. Pöschel, *Kinetic Theory of Granular Gases* (Oxford University Press, Oxford, 2003).
[3] T. Pöschel and T. Schwager, *Computational Granular Dynamics, Models and Algorithms* (Springer, New York, 2005).
[4] F. Cajori, *Newton's Principia—A Revision of Mott's Translation* (University of California Press, Berkeley, 1934).
[5] E. Hodgkinson, J. Franklin Inst. **19**, 140 (1835).
[6] P. G. Tait, Trans. R. Soc. Edinburgh **36**, 225 (1892).
[7] G. Barnes, Am. J. Phys. **26**, 5 (1958).
[8] G. Barnes, Am. J. Phys. **26**, 9 (1958).
[9] S. F. Foerster, M. Y. Louge, H. Chang, and K. Allia, Phys. Fluids **6**, 1108 (1994).
[10] L. Labous, A. D. Rosato, and R. N. Dave, Phys. Rev. E **56**, 5717 (1997).
[11] M. Y. Louge and M. E. Adams, Phys. Rev. E **65**, 021303 (2002).
[12] F. G. Bridges, A. Hatzes, and D. N. C. Lin, Nature **309**, 333 (1984).
[13] J. M. Lifshitz and H. Kolsky, J. Mech. Phys. Solids **12**, 35 (1964).
[14] G. Kuwabara and K. Kono, Jpn. J. Appl. Phys. **26**, 1230 (1987).
[15] W. Tabakoff, J. Propul. Power **7**, 805 (1991).
[16] C. J. Reagle, J. M. Delimont, W. F. Ng, S. V. Ekkad, and V. P. Rajendran, Meas. Sci. Technol. **24**, 105303 (2013).
[17] A. P. R. Wadlund, Am. J. Phys. **7**, 194 (1939).
[18] C. V. Raman, Phys. Rev. **12**, 442 (1918).
[19] I. Stensgaard and E. Lægsgaard, Am. J. Phys. **69**, 301 (2001).
[20] A. D. Bernstein, Am. J. Phys. **45**, 41 (1977).
[21] M. Ciocca and J. Wang, J. Ky. Acad. Sci. **72**, 100 (2011).
[22] C. E. Aguiar and F. Laudares, Am. J. Phys. **71**, 499 (2003).
[23] T. C. Ribeiro, J. F. A. Romero, and J. A. A. Romero, ABCM Symp. Ser. Mech. **5**(Sec. III.11), 676 (2012).
[24] A. Wadhwa, Phys. Educ. **47**, 620 (2012).
[25] P. A. Smith, C. D. Spencer, and D. E. Jones, Am. J. Phys. **49**, 136 (1981).
[26] A. Wadhwa, Phys. Educ. **44**, 517 (2009).
[27] S. K. Foong, D. Kiang, P. Lee, R. H. March, and B. E. Paton, Phys. Educ. **39**, 40 (2004).
[28] J. Nunn, Phys. Educ. **49**, 303 (2014).
[29] K. C. Maynes, M. G. Compton, and B. Baker, Phys. Teach. **43**, 352 (2005).
[30] J. Wang and M. Ciocca, Phys. Teach. **50**, 503 (2012).
[31] M. Leconte, Y. Garrabos, F. Palencia, C. Lecoutre, P. Evesque, and D. Beysens, Appl. Phys. Lett. **89**, 243518 (2006).
[32] M. G. Koller and H. Kolsky, Int. J. Solids Struct. **23**, 1387 (1987).
[33] E. Falcon, C. Laroche, S. Fauve, and C. Coste, Eur. Phys. J. B **3**, 45 (1998).
[34] H. King, R. White, I. Maxwell, and N. Menon, Europhys. Lett. **93**, 14002 (2011).
[35] G. C. McLaskey and S. D. Glaser, J. Acoust. Soc. Am. **128**, 1087 (2010).
[36] R. Sondergaard, K. Chaney, and C. E. Brennen, J. Appl. Mech. **57**, 694 (1990).
[37] P. Müller, M. Heckel, A. Sack, and T. Pöschel, Phys. Rev. Lett. **110**, 254301 (2013).
[38] J. R. Taylor, *An Introduction to Error Analysis: The Study of Uncertainties in Physical Measurements* (University Science Books, Mill Valley, CA, 1997), 2nd ed.
[39] P. Timmerman and J. P. van der Weele, Am. J. Phys. **67**, 538 (1999).
[40] M. Montaine, M. Heckel, C. Kruelle, T. Schwager, and T. Pöschel, Phys. Rev. E **84**, 041306 (2011).
[41] N. V. Brilliantov, F. Spahn, J.-M. Hertzsch, and T. Pöschel, Phys. Rev. E **53**, 5382 (1996).
[42] T. Schwager and T. Pöschel, Phys. Rev. E **57**, 650 (1998).
[43] T. Schwager and T. Pöschel, Phys. Rev. E **78**, 051304 (2008).
[44] R. Ramírez, T. Pöschel, N. V. Brilliantov, and T. Schwager, Phys. Rev. E **60**, 4465 (1999).
[45] P. Müller and T. Pöschel, Phys. Rev. E **84**, 021302 (2011).
[46] N. Gunkelmann, M. Montaine, and T. Pöschel, Phys. Rev. E **89**, 022205 (2014).
[47] A. Glielmo, N. Gunkelmann, and T. Pöschel, Phys. Rev. E **90**, 052204 (2014).
[48] A. Lorenz, C. Tuozzolo, and M. Y. Louge, Exp. Mech. **37**, 292 (1997).
[49] A. Hatzes, F. G. Bridges, and D. N. C. Lin, Mon. Not. R. Astron. Soc. **231**, 1091 (1988).
[50] C. M. Sorace, M. Y. Louge, M. D. Crozier, and V. H. C. Law, Mech. Res. Comm. **36**, 364 (2009).